THE JOURNAL OF PHYSICAL CHEMISTRY C
A JOURNAL OF THE AMERICAN CHEMICAL SOCIETY

pubs.acs.org/JPCC

Article

In Operando FTIR Study on the Effect of Sulfur Chain Length in Sulfur Copolymer-Based Li−S Batteries

Ayda Rafie, Rhyz Pereira, Ahmad Arabi Shamsabadi, and Vibha Kalra*

Cite This: *J. Phys. Chem. C* 2022, 126, 12327−12338

Read Online

ACCESS | Metrics & More | Article Recommendations | Supporting Information

ABSTRACT: Synthesis of sulfur-rich copolymers using the inverse vulcanization reaction is a practical approach to modify the sulfur active material for enhanced stability in Li−S batteries. However, to effectively design such polymers, a thorough understanding of the underlying redox mechanisms is critical. Here, we study electrochemical behavior of sulfur-rich copolymers using *in operando* FTIR spectroscopy with attenuated total reflection. We used sulfur-diisopropenylbenzene copolymers [poly(S-*co*-DIB)] as the active material in Li−S batteries and monitored the evolution of the C−S peak position and cyclic changes in the S−S bond stretching at different potentials during discharge and charge. Moreover, we synthesized various copolymers with sulfur wt % of 80 and 30 wt % and compared the electrochemical behavior and their corresponding IR response during cyclic voltammetry sweep. Our results indicated that the C−S bond in sulfur copolymers is not active in the voltage window of Li−S batteries. Moreover, we showed that the shift in the C−S peak position becomes smaller with increase in the monomer wt %. In addition, the S−S stretching peak at ∼500 cm^{-1} diminishes when the sulfur wt % is decreased from 80 to 30 wt %, highlighting a significant change in electrochemical behavior of the copolymers.

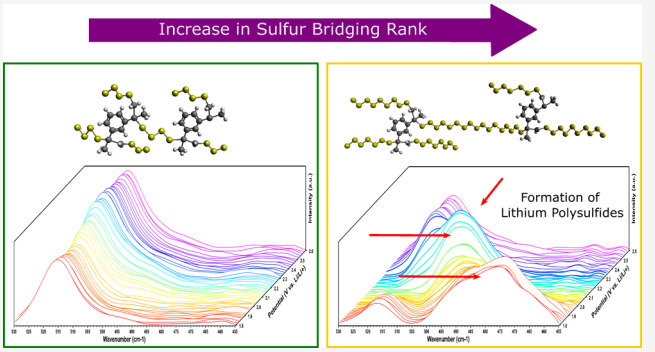

INTRODUCTION

Lithium−sulfur (Li−S) batteries are considered as the next candidate for commercialization in the battery industry. The advantages of Li−S batteries arise from sulfur as the active material, which has a high theoretical discharge capacity (∼1675 mA h/g) and is cheap, abundant, and environmentally friendly.[1,2] Despite all advantages of these batteries, there are several challenges in achieving long-term cycling. The challenges on the sulfur cathode side are (a) the insulating nature of sulfur (S_8), the initial active material, and Li_2S, the discharge product, (b) volume expansion of ∼80% in each discharge, and (c) formation of soluble lithium polysulfides during sulfur reduction, resulting in notorious polysulfide shuttling.[3−5] Among these challenges, polysulfide shuttling is known to be the most prominent reason behind the poor performance and cycle life of Li−S batteries.[1,3] To address this challenge, several studies have focused on cathode modifications[6] and electrolyte,[7−9] interlayer,[10] and separator[11,12] design. Reports on sulfur cathodes largely involve development of porous host materials[7,13,14] or other sophisticated material design to enhance the conductivity of the cathode,[15,16] accommodate volume expansion,[17,18] and most importantly to physically and/or chemically entrap the lithium polysulfides to prevent their shuttling.[19−22]

An alternate approach in mitigating polysulfide shuttling is active sulfur modification through the formation of S−X bonds, where X can be carbon,[23,24] phosphorus,[25] or Se/Te.[6,26,27] To this end, Pyun et al. introduced the inverse vulcanization reaction as a facile method to synthesize sulfur-rich copolymers with varying sulfur contents.[28,29] In 2014, the same group, for the first time, investigated the application of such sulfur-rich copolymers, specifically, sulfur-diisopropenylbenzene copolymers [poly(S-*co*-DIB)] (SDIB) as an active material in Li−S batteries.[30] Following this study, several attempts have been made to combine the SDIB copolymer with various host materials such as carbon nanotubes,[31] graphene sheets,[32] and onion-like carbons.[33] Other literature reports used the inverse vulcanization reaction with different monomers to synthesize various types of copolymers to be used as an active material in Li−S batteries.[30,34−39] While inverse vulcanization gives lower capacities than pure sulfur, the improved cycling stability via polysulfide mitigation is thought to be a worthwhile trade-off.[30] The focus of most reports has been to enhance the performance of Li−S batteries with little understanding of the mechanism and/or correlations between the copolymer composition/properties on electro-

Received: October 20, 2021
Revised: May 4, 2022
Published: July 21, 2022

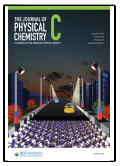

https://doi.org/10.1021/acs.jpcc.1c09124
J. Phys. Chem. C 2022, 126, 12327−12338

chemical behavior. Few studies have employed *postmortem* experiments, where the battery is stopped at a specific depth of discharge and the cathode material is retrieved for analysis. However, due to possible exposure to air and the strong dependence of intermediate species on the potential of Li−S batteries, the *postmortem* results may not provide an accurate representation.[40,41] Moreover, the underlying assumption in most work on sulfur-rich copolymers has been that sulfur is immobilized through the formation of the C−S bond in the active material, thereby forming "bound" organo-lithium polysulfides instead of "loose" polysulfides during discharge, preventing shuttle.[31,37] In other words, the organic moieties have been hypothesized in the literature to perform as anchors and stabilize the polysulfides formed during discharge, which otherwise would dissolve in the electrolyte and diffuse to the anode side.

In our recent study,[42] we demonstrated that microporosity of the cathode host, which is known to physically confine conventional "loose polysulfides," still plays a profound role in enhancing the cycle stability of the SDIB-based copolymers, alluding to the fact that loose polysulfides are indeed present in the system and therefore still benefit from entrapment into tiny pores. As a part of that study, we discussed that despite the C−S covalent bond in the initial active material, that is, SDIB or other sulfur-rich copolymers, the formation of loose polysulfides is inevitable. This is due to the possibility of multiple S−S bond cleavages during discharge owing to the long sulfur bridging chains between the monomers—typically 8−10 atom-long in the 80−90% sulfur content polymers, C−S−S_n−S−C, which on charging may form loose sulfur, S_8. In other words, the sulfur-rich copolymers do not completely eliminate polysulfides; instead, they only delay the formation of polysulfides.

Motivated by this understanding, we have systematically investigated the effect of sulfur chain length on the electrochemical behavior of sulfur-rich copolymers using *in operando* Fourier transform-infrared spectroscopy with attenuated total reflection (FTIR-ATR). Specifically, we synthesized four SDIB copolymers with varying sulfur bridging chain lengths by tuning the sulfur wt % from 90 to 30 wt % during inverse vulcanization. We refer to these copolymers as S90DIB10, S80DIB20, S50DIB50, and S30DIB70. TGA, XRD, and DSC characterizations show a significant change in the copolymer crystalline structure, and thermal properties when the sulfur wt % is less than 50 wt %.

We hypothesize that decreasing the sulfur chain length (i.e., sulfur wt % in the copolymer) would result in different electrochemical behaviors. Shorter sulfur chain lengths should lead to the formation of fewer polysulfides, leading to slower capacity fade. To validate our hypothesis, we conducted standard electrochemical characterizations such as cyclic voltammetry (CV) and *in operando* FTIR to monitor chemical changes in real time during battery cycling. CV scans confirmed that the first discharge peak at ∼2.3 V in S80DIB20, which corresponds to formation of high-order polysulfides and organo-polysulfides from S_8 and SDIB, respectively, weakened in S50DIB50 and completely disappeared when the sulfur wt % was decreased to 30 wt % in S30DIB70. Following electrochemical characterization, we built an *in operando* FTIR cell to study the evolution of the C−S bond representing the organo-lithium polysulfides and S−S bond representing the polysulfides. The *in operando* cell assembly closely replicated a coin cell without altering the key battery components, such as electrolyte volume, cathode, sulfur loading, and so forth, which was made possible using the ATR accessory. Via this spectro-electrochemical investigation, we found that the C−S peak is not active in the potential window of Li−S batteries, contrary to the hypothesis presented in several previous papers on sulfurized polyacrylonitrile sulfur copolymers.[43−46] Moreover, during discharge, the shift in the C−S bond peak position is smaller when the sulfur wt % is decreased, confirming that the change in sulfur chain length during reduction is less significant in the S30DIB70 copolymer due to a shorter initial sulfur bridge length. While we observed clear peaks for higher-order polysulfides and polysulfide evolution in the higher-sulfur-bridge-length copolymer, S80DIB20, during discharge (and charge), no polysulfide peak was seen for the low-sulfur-bridge-length copolymer, S30DIB70. These results confirm that by decreasing the sulfur wt %, and subsequently decreasing the sulfur chain length, a different electrochemical behavior is observed.

This work is the first study to employ *in operando* investigation of sulfur copolymers to systematically investigate the effect of sulfur chain length on the electrochemical reaction pathways. We believe that these results can advance the optimization of materials with S−X bond, which can immobilize sulfur and enhance the cycling performance of Li−S batteries.

EXPERIMENTAL METHODS

Copolymer Synthesis and CNF Fabrication. Inverse vulcanization was used to synthesize the sulfur-rich copolymers with various monomer wt %, as reported by Chung et al.[28] All reactions were carried out in an oil bath at 185 °C and inside a fume hood to avoid any possible H_2S exposure. To prepare the SDIB powders, sulfur (Sigma, 100 mesh) was melted until an orange color was observed; then, an appropriate amount of the 1,3-diisoprpenylbenzene monomer (DIB, TCI) was added, followed by stirring until a deep-red color was observed. The amount of sulfur, DIB, and reaction time for preparing each copolymer is presented in Table1.

Table 1. Amounts of Sulfur and DIB and Reaction Time for Synthesis of Copolymers

copolymer	sulfur amount (g)	DIB amount (g μL)
S90DIB10	2.7	0.30−325
S80DIB20	2.7	0.67−732
S50DIB50	2.7	2.70−2927
S30DIB70	2.0	4.67−5059

The copolymers were given the identifier S*x*DIB*y* to identify the wt % of sulfur and the monomer used in the synthesis reaction, with *x* being the wt % of sulfur and *y* being the wt % of monomer. The reaction yielded a block of red transparent material which was cooled to room temperature, removed from the reaction vials, and further ground. To grind the copolymers, we used liquid nitrogen to decrease the copolymer temperature below the glass transition temperature (T_g), and we manually ground them into powders. Figure S1, in the Supporting Information, shows digital photos of the copolymer powders. As can be seen in the images, by decreasing the sulfur wt %, the copolymers became darker in color. We used electrospinning to synthesize the carbon nanofibers (CNFs). In this technique, a polymeric solution was made using polyacrylonitrile (PAN, average MW: 150,000, Sigma-Aldrich)

https://doi.org/10.1021/acs.jpcc.1c09124
J. Phys. Chem. C 2022, 126, 12327−12338

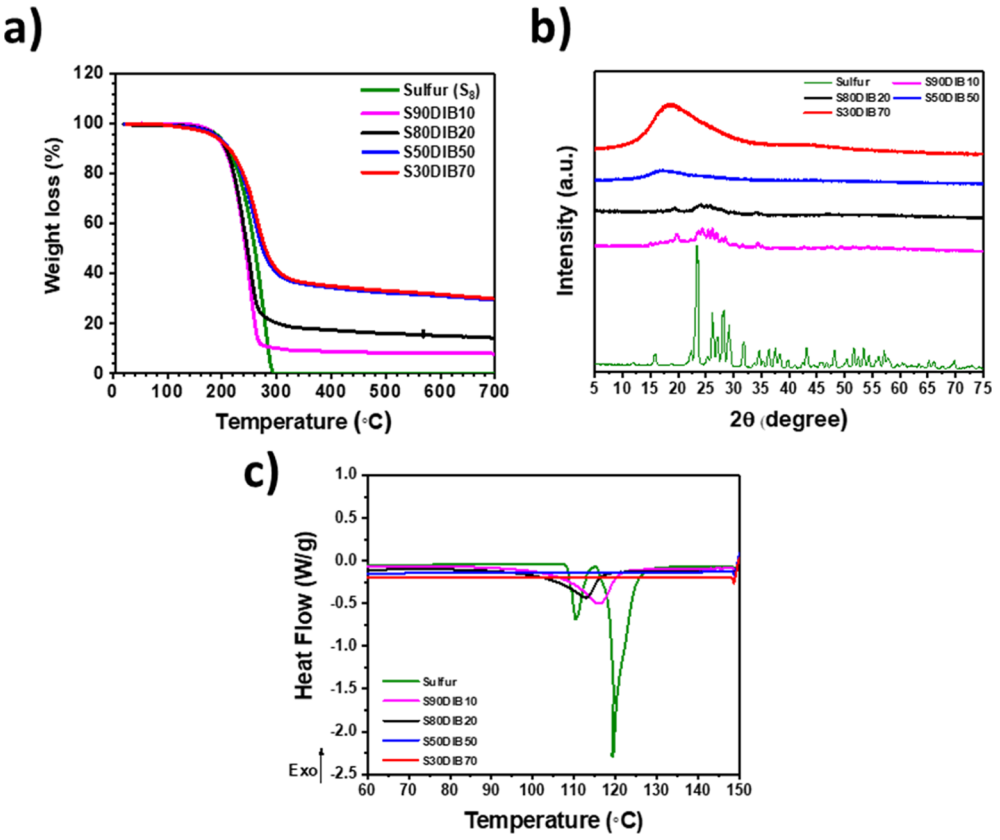

Figure 1. (a) TGA result of copolymers, (b) XRD result of copolymers with various sulfur/monomer wt %, and (c) DSC result of copolymers with various sulfur wt % in the first heating cycle.

and dried LIQUION (Nafion, Liquion 1105, Ion Power Inc.) in the ratio of 40:60 wt % in *N*,*N*-dimethylformamide (DMF, Sigma-Aldrich) solvent. The solid concentration was 18 wt %/in the solution. This polymer was stirred overnight at 60 °C and was loaded into a syringe using a 22-gauge needle (stainless-steel needle, Hamilton Co.) immediately after. The electrospinning parameters were as follows: the flow rate of the syringe pump (New Era Pump Systems, Inc.) was set to 0.2 mL/h, the distance between the grounded Al collector and needle was adjusted between 15 and 16 cm, the humidity inside the chamber was controlled to be <20%, and the applied voltage was adjusted between 8 to 10 kV to ensure smooth and beadless spinning. Each electrospinning experiment was carried out for ∼6 h. The resulting electrospun mats were collected and stabilized at 280 °C in air for 6 h using a convention oven (Binder Inc, Germany). Following the stabilization process, the CNFs were transferred to a tube furnace (MTI Co., USA), where they were pyrolyzed at 1000 °C for 1 h under continuous N_2 flow. The heating rate of the furnace was set to 3 °C/min to reach from room temperature to 1000 °C, and a similar cooling rate was maintained for cooling down the furnace from 1000 to 200 °C.

Physical Characterization of the Samples. To evaluate the morphology of the CNFs, copolymers, and cathode, scanning electron microscopy (Zeiss Supra, 50 VP) was employed. The qualitative and quantitative elemental analysis were conducted using an energy-dispersive spectrometer (Oxford), coupled with a scanning electron microscope. To increase the conductivity of the samples, they were coated with an ultrathin layer of platinum using a sputter coater (Cressington) before transferring them to the scanning electron microscope chamber. To determine the composition of sulfur and sulfur copolymers, thermogravimetric analysis (TGA) was carried out using a TA 2950 (TA Instruments, USA), under a steady-state continuous flow of N_2. The TGA experiments were carried out from room temperature to 700 °C at a heating rate of 5 °C/min. To evaluate the thermal properties of the samples, differential scanning calorimetry (DSC) was performed using a Q-2000 (TA instruments) calorimeter. The heating and cooling rates were adjusted to 10 °C/min. The samples were first heated to 150 °C to omit all thermal history. Following this step, the samples were cooled down to −90 °C using liquid nitrogen and heated up to 150 °C, under nitrogen flow. This procedure was repeated three times. X-ray diffraction (XRD) was carried out using a Rigaku Miniflex 600, without any modification of the samples. The infrared spectra of the copolymers were obtained using a Fourier transform infrared (FTIR) spectrometer (Nicolet iS50, Thermo-Fisher Scientific), equipped with an extended range diamond ATR accessory and with a deuterated triglycine sulfate (DTGS) detector. The spectra were collected with a resolution of 64 scans per spectrum at 8 cm^{-1}, and they were corrected using background, baseline, and advanced ATR corrections in the Thermo Scientific Omnic software package. The structures of the copolymers in schematics were generated using Avogadro software.[47]

Cell Fabrication and Electrochemical Testing Procedures. In this study, we used the CNFs as the host material and sulfur-rich copolymers as the active material. Before cathode preparation, the CNF mats were punched into 0.855 cm^2 disks and dried at 140 °C in a convection oven overnight. We used the "ultrarapid melt diffusion" technique, previously

https://doi.org/10.1021/acs.jpcc.1c09124
J. Phys. Chem. C 2022, 126, 12327−12338

developed in our lab,[48] to diffuse the copolymer powders into electrospun CNFs; these samples are referred to as CNF/S*x*DIB*y*. In this technique, the desired amount of copolymer is sprinkled onto the CNFs and subsequently heated at 155 °C for 2 min using a hot press, applying very slight pressure. These cathodes were transferred inside a glovebox (O_2 and H_2O < 1 ppm) after drying overnight under vacuum inside the glovebox antechamber. The CNF/S*x*DIB*y* cathodes were used without any further modification or any need for the current collector. We used CR2032 coin cells with stainless-steel spacers and springs (all purchased from MTI Co), Li foil (Aldrich, punched to 13 mm diameter discs) as the anode, and a polypropylene separator (Celgard 2500; 19 mm diameter). The electrolytes used in all cells are conventional ether-based electrolytes, with 1.85 M $LiCF_3SO_3$ (99.995% trace-metal basis, Sigma Aldrich) salt and 0.1 M $LiNO_3$ (Acros Organics) additive in a mixture of 1,2-dimethoxyethane (DME, Acros Organics) and 1,3-dioxolane (DOL, Sigma-Aldrich) solvents, mixed at a 1:1 volume ratio. The additive and salt were transferred to the glovebox upon receiving without any modification. The amount of electrolyte used in the coin cells was 30 μL. The fabricated Li−S coin cells were rested for 4 h and were conditioned at C/10 and C/5 cycles (two cycles each) prior to long-term cycling at C/2, where 1C = 1675 mA h/g. The long-term stability of these coin cells was tested by a galvanostatic charge−discharge experiment in a Li−S battery potential window of 1.8−2.7 V (vs Li/Li^+) using a Maccor cycler (4000 series). The discharge capacity of the cells was calculated based on the weight of sulfur. The CV measurements were carried out using a Gamry (reference 1000) potentiostat.

***In Operando* FTIR Cell Assembly and Electrochemical Testing.** To build the *in operando* FTIR cell, we transferred the FTIR puck to an argon-filled glovebox and the coin cell assembly was replicated on the extended range diamond crystal. For this cell, we used 45 μL of the electrolyte, the cathode (CNFs, SCNFs, S80DIB20/CNFs, and S30DIB70/CNFs), a Celgard separator, and a Li metal anode (10 mm disc). The stainless-steel spacer was replaced with a trilayer Ni foam (MTI Co). The cell was sealed using a coin cell top, vacuum grease, and a Kapton tape. The *in operando* cell was then transferred outside the glovebox and was connected to a Gamry reference 1000 potentiostat. The stainless-steel puck was used as the current collector for the cathode, and an Al foil strip was attached to the top of the coin cell to connect the *in operando* cell to the Gamry potentiostat. We used the pressure anvil on the FTIR instrument to apply pressure to the cell and ensure a good contact inside the cell. For collecting CVs, we first rested the cell for 1 h at an open-circuit potential. The CVs were collected at a scan rate of 0.02 mV/s between 1.8 and 2.7 V (vs Li/Li^+) for three cycles. The collected series were then analyzed using macros in the Omnic software package, and each spectrum was corrected using background, baseline, and advanced ATR corrections, as explained before.

RESULTS AND DISCUSSION

Sulfur-Rich Copolymer Characterization and Electrochemical Behavior. The sulfur-rich copolymers with 90, 80, 50, and 30 wt % of sulfur were synthesized using the inverse vulcanization reaction. To identify these polymers, throughout the article, we have used S*x*DIB*y*, where *x* and *y* are wt % of sulfur and the monomer, respectively, and $y = 100 - x$. Figure 1a shows the TGA results for these polymers from room temperature to 700 °C. As can be seen in this figure, the onset temperature for sulfur decomposition does not change upon changing the sulfur wt % in the copolymers. Based on these results, the wt % of sulfur in the copolymers for S80DIB20 and S90DIB10 can be confirmed using TGA. However, the weight loss % of S50DIB50 and S30DIB70 nearly overlap. In both of these copolymers, a ∼60% weight loss was observed. Although similar results have been reported in the literature for sulfur copolymers containing 50 wt % of sulfur,[35] no possible explanation is provided. This behavior might be related to formation of a stronger C−S peak in these copolymers, which prevents the decomposition of the C−S bond and sulfur evaporation in these copolymers. In order to confirm the sulfur weight % in these copolymers, we further conducted scanning electron microscopy (SEM) and energy-dispersive X-ray spectroscopy (EDS) on these copolymers (Figure S2). Based on the results (Table S1), the sulfur contents of S50DIB50 and S30DIB70 are ∼53.89 and ∼31.41 wt %, respectively, which are very close to the wt % used for the reactions, as described earlier in the Experimental Methods section.

To characterize the crystalline structure of the copolymers, XRD spectra of the copolymers were collected, and the results were compared with that of pure sulfur powder (Figure 1b). The XRD results showed a significant difference between the crystalline structure of these copolymers with decreasing sulfur wt % (i.e., increasing monomer wt %). The S90DIB10 and S80DIB20 samples show a semicrystalline structure, and some crystalline sulfur peaks are present. This can be attributed to the existence of unreacted (not bound to carbon) sulfur or can be simply a result of long-chain bridging sulfur that is not terminated with carbon. This means that the sulfur atoms in long-chained copolymers can undergo the unzipping process mentioned previously in ref 49. For S50DIB50 and S30DIB70 copolymers, a completely amorphous material is observed. XRD also confirms that a significant change in the copolymer properties occurs when the sulfur wt % decreases to 50 and 30 wt %. Figure 1c shows the DSC curves of the SDIB copolymers and sulfur (S_8) powder as the reference. The samples were first heated up to 150 °C, then cooled down to −90 °C, and again heated to 150 °C. This experiment was repeated for 3 cycles, and Figure 1c shows the result of the first heating cycle. The sulfur powder shows two melting peaks at 110 and 119 °C. The first peak at 110 °C can be ascribed to the solid−solid transition of sulfur from the orthorhombic crystal to the monoclinic crystal, The second peak is the solid−liquid melting peak at 119 °C. In the following cycles, however, only one melting peak at ∼120 °C was observed.[49] The copolymers S90DIB10 and S80DIB20 also show a small melting peak at ∼116 and ∼112 °C, respectively. These melting peaks disappear in the subsequent heating cycles shown in the Supporting Information (Figure S3a,b). This indicates that the unreacted sulfur could polymerize with the DIB monomer in the first heating cycle. Similar results are also reported in ref 49. Moreover, the T_g values of the copolymers were obtained from the DSC curves. The T_g values of −12, −7, 21, and 28 °C were obtained for S90DIB10, S80DIB20, S50DIB50, and S30DIB70 copolymers, respectively. The DSC results show that the T_g of the copolymer increases with decreasing sulfur chain length. The presence of melting peaks in the DSC curves of S90DIB10 and S80DIB20 but the absence of the melting peaks in S50DIB50 and S30DIB70 could be related to the presence of a small amount of unreacted sulfur. This could be a result of the unzipping process explained before. On the other

https://doi.org/10.1021/acs.jpcc.1c09124
J. Phys. Chem. C 2022, 126, 12327−12338

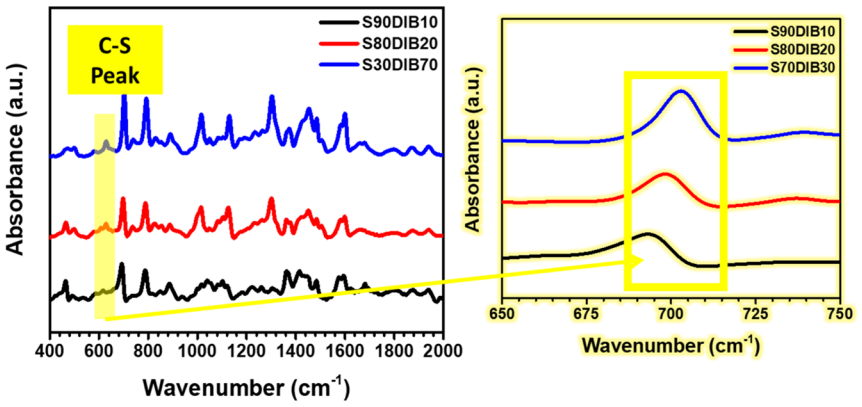

Figure 2. FTIR result of copolymers with the C−S peak region highlighted in yellow.

hand, the absence of the melting peak confirms the complete crosslinking and transformation to amorphous material in the case of S50DIB50 and S30DIB70 copolymers. Based on the XRD and DSC results, we can confirm that there is no loose sulfur in the S50DIB50 and S30DIB70 copolymers, and the sulfur chain lengths in these copolymers are significantly shorter than those of S90DIB10 and S80DIB20.

To confirm the formation of the C−S bond in the copolymers, we conducted FTIR spectroscopy. The result of these experiments is shown in Figure 2. The peaks at 692 cm^{-1} correspond to the C−S bond, and the peak at 465 cm^{-1} is attributed to the S−S bond in these copolymers. As a reference, we have the S−S peak in elemental sulfur at ∼464 cm^{-1}. It is worth mentioning that the C−S peak at 692 cm^{-1} for S90DIB10 shifts to higher wavenumbers when the sulfur wt % decreases from 90 to 80, 50, and 30 wt %. A possible explanation for such shift in the C−S peak position is the decrease in sulfur chain length.

To evaluate the electrochemical behavior of these copolymers, we fabricated cathodes with electrospun CNFs as the host material and sulfur copolymers with varying sulfur wt % as the active material. We used the ultrarapid hot-press-assisted melt diffusion technique, previously developed by our lab, as a simple method to diffuse copolymers into the CNF host.[48] Figure 3 shows the representative SEM for two different cathodes—S80DIB20/CNFs and S30DIB70/CNFs. Based on the SEM pictures, the copolymer is well distributed throughout the CNF host material.

Figure 4 shows the CV scans of the cathodes made from S80DIB20, S50DIB50, and S30DIB70. The details of cathode fabrication can be found in our previous report.[42] As can be seen in the figure, when S80DIB20 powder is used, two reduction peaks at ∼2.3 and ∼2.0 V appear, which represent the formation of higher- and lower-order lithium polysulfides and lithium organo-polysulfides. Lower-order polysulfides are defined as Li_2S_x (x = 1, 2) for the purpose of this study in order to differentiate them from their more soluble counterparts. These peaks are similar to sulfur reduction peaks at ∼2.3 and 2.0 V shown in Figure S4. Upon decreasing the sulfur concentration from 80 to 50%, the intensity of the 2.3 V reduction peak decreases significantly, implying that the formation of high-order polysulfides and high-order organo-polysulfides is reduced. With further decrease in the sulfur wt % to 30 wt %, the reduction peak at ∼2.3 V disappears. The disappearance of the peak at ∼ 2.3 V suggests that the formation of high-order lithium polysulfides is avoided, which

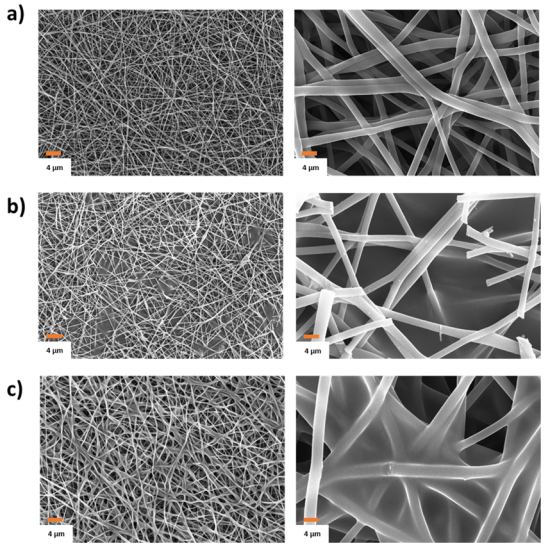

Figure 3. SEM pictures of (a) CNFs, (b) S80DIB20I/CNFs, and (c) S30DIB70/CNFs used as cathodes in coin cells and *in operando* cells.

we believe is attributed to the existence of a short sulfur bridge chain length in S30DIB70 (Figure 4). Cathodes using S80DIB20 and S30DIB70 were fabricated into coin cells and were cycled at C/2. Cycling performance (Figure S8) shows that lower weight percentage of sulfur yields much more stable capacities, while higher weight percentages showed much more capacity fade. This suggests that a higher-sulfur-percentage active material is much more susceptible to polysulfide formation. On the other hand, the S30DIB70 cathode shows a much better cycle life (over 1500 cycles). It is also important to note that the capacity of the S30DIB70 active material is significantly lower than that of S80DIB20. This arises from the lower sulfur chain length of the S30DIB70 active material. To test our hypothesis, we designed *in operando* FTIR cells and monitored the C−S bond an S−S bond (in polysulfides) in real time during battery cycling for copolymers with varying sulfur wt %.

***In Operando* Spectro-Electrochemical Investigation of Sulfur-Rich Copolymers in Li−S Batteries.** Figure 5 shows the scheme for the *in operando* cell designed in our lab.[50] It is worth mentioning that the facile design of the operando cells used in this study has two important and unique features. The first one is the ATR accessory used, which also acts as a positive current collector. The second feature is the

https://doi.org/10.1021/acs.jpcc.1c09124
J. Phys. Chem. C 2022, 126, 12327−12338

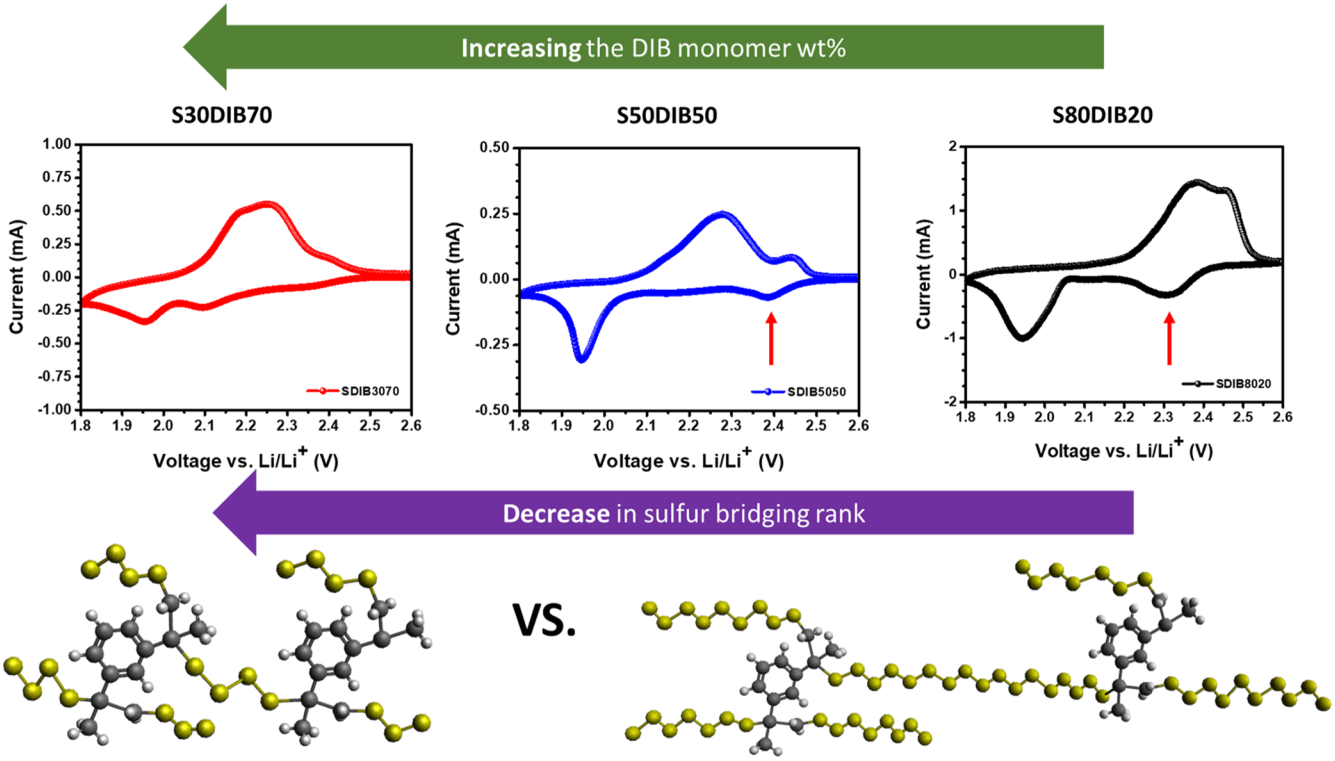

Figure 4. Cyclic voltammograms of S80DIB20, S50DIB50, and S30DIB70 copolymers and a schematic showing the change in the chemical structure of the copolymers with increasing monomer wt %, which results in a decrease of the sulfur chain length.

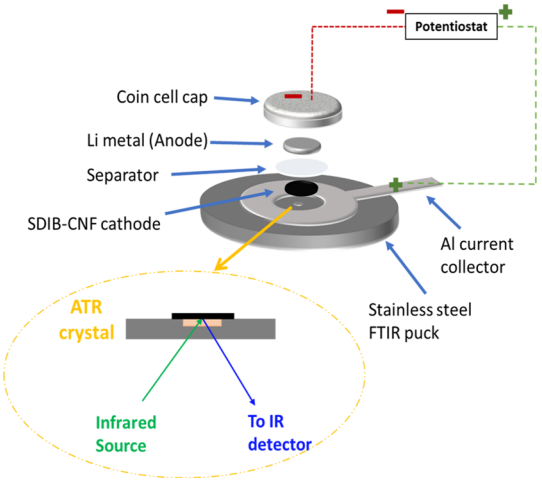

Figure 5. Setup used for in situ experiments with an extended diamond on the ATR accessory.

free-standing CNF mat used as a sulfur host, which does not require the addition of binders and can be used without the Al current collector, which would otherwise block the IR spectrum and prevent the collection of appropriate intensity signals. The *in operando* cell assembly, geometry, and parameters (including electrolytes) mimic actual coin cell batteries used for testing Li−S cell performances. Figure S5a,b in the Supporting Information shows the CV and FTIR spectra obtained for a blank cell, respectively. A blank battery cell is a cell without any sulfur-based active material, and the cathode used in these cells is only the CNF. The CV results confirm that the electrolyte does not contribute to any capacity in the cells. Moreover, the FTIR spectra of the blank cells show that the FTIR peaks of the electrolyte do not shift with change in the cell potential. Therefore, any changes to be seen in the FTIR spectra of the SDIB-based Li−S cell during cycling will be solely due to the changes in bands of the active material.

As the next step, we selected two copolymers with significantly varying sulfur wt % for *in operando* IR studies—S80DIB20 and S30DIB70. Previous studies such as *ex situ* NMR study and other reports in refs 51 and 52 showed that decreasing sulfur wt % in an inverse vulcanization reaction results in formation of copolymers with a lower sulfur bridging rank. Based on the XRD, DSC, and FTIR results, we observed significant differences between the crystalline structure and thermal properties of these copolymers. Therefore, for the *in operando* cell, we decided to use S80DIB20 and S30DIB70 copolymers, which represent copolymers with a high-sulfur chain length and low-sulfur chain length, respectively. As reference, Figure 6 shows the FTIR spectra for the blank cell and a representative SDIB cell at both open-circuit voltage (OCV) and at 2.3 V. We label two relevant fingerprint regions that we carefully monitored and evaluated via *in operando* spectroscopy as we discharged and charged the cell for three cycles—(1) region around ∼695 cm^{-1}, highlighted in purple, representing the C−S vibration from the copolymer, and (2) region around ∼500 cm^{-1}, highlighted in orange, representing the S−S stretching from polysulfides. As seen in Figure 6, the peaks in these regions do not interfere with any peaks from our electrolyte (shown in the blank cell).

***In Operando* IR Study on Evolution of the C−S Vibration in Sulfur Copolymers.** We first focus on the evolution of the C−S peak as a function of cell potential. Figure 7a shows the CV data collected *in operando*/during cell cycling for the S80DIB20 copolymer, and Figure 7b presents the corresponding IR spectra between 685 to 710 cm^{-1} during discharge in the first cycle. We see a clear blue shift in the C−S

https://doi.org/10.1021/acs.jpcc.1c09124
J. Phys. Chem. C 2022, 126, 12327−12338

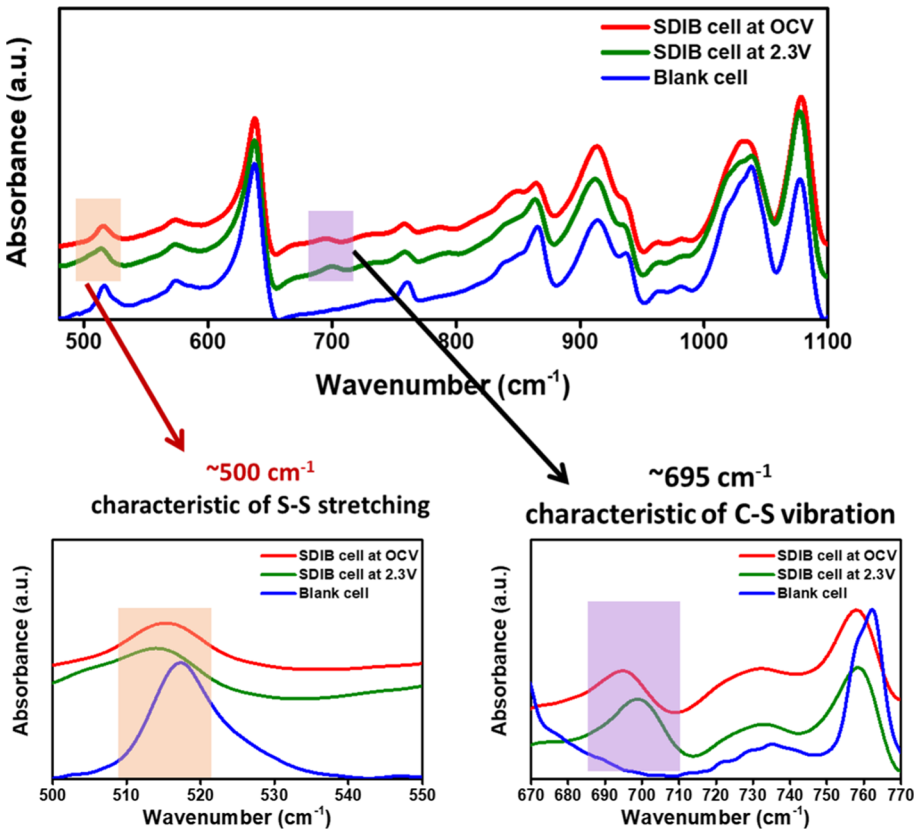

Figure 6. FTIR spectra of the blank cell (without any active material) compared to the copolymer cell at OCV and 2.3 V with the C−S peak (purple region) and S−S peak regions (orange region) zoomed in.

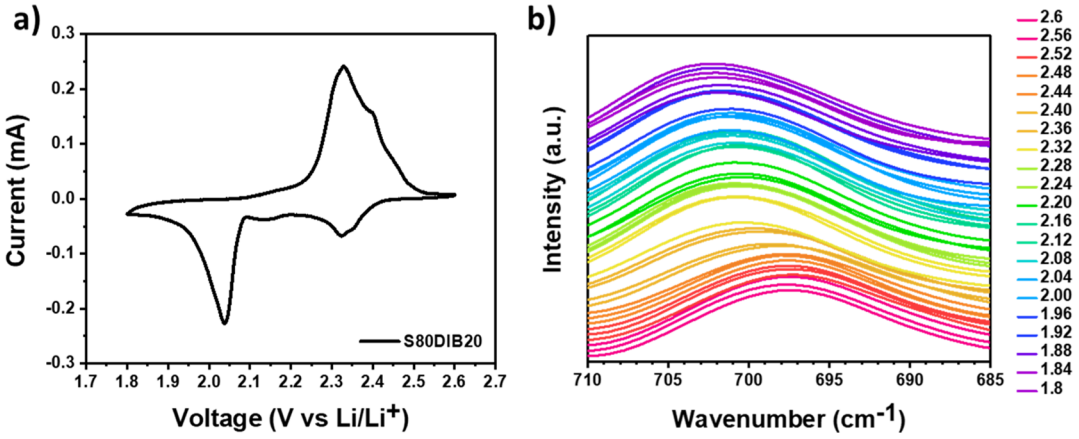

Figure 7. CV of the in situ cell with the S80DIB20 copolymer active material and (b) C−S region in the FTIR spectra collected simultaneously.

peak position of S80DIB20 as the cell is discharged from 2.7 to 1.8 V. We believe that this shift can be attributed to the lithiation of the organic moiety of the copolymer and decrease in sulfur chain length during discharge. In other words, the formation of C−S−...−Li (lithium organo-polysulfides) with various sulfur chain lengths at different depths of discharge (DODs) is responsible for the changes in the C−S peak position. This can be explained by looking at the electronegativity numbers of the atoms involved. As the cell is discharged, Li cation-terminating ions with lower electronegativity (∼0.98), compared to sulfur (electronegativity: ∼2.58), become closer to the C−S peak in the copolymer. As a result, the C−S peak becomes stronger and shifts toward higher wavenumbers.

Another important conclusion from this figure is that the C−S peak does not disappear during the discharge process, and therefore, we can conclude that the C−S peak in sulfur-rich copolymers is not electrochemically active in the potential window of Li−S batteries, that is, 1.8−2.7 V versus Li/Li^+. It is worth noting that this is the first ever study demonstrating the evolution of the polymeric structure in sulfur-rich copolymers during battery operation. Some studies have suggested that the C−S bond of the sulfur copolymeric active material breaks during the discharge and re-forms during charge.[24,53] These studies have proposed following electrochemical reactions for such copolymers

$$RSS_nSR + 2(n+2)Li^+ \leftrightarrow 2R + (n+2)Li_2S \quad (1)$$

https://doi.org/10.1021/acs.jpcc.1c09124
J. Phys. Chem. C 2022, 126, 12327−12338

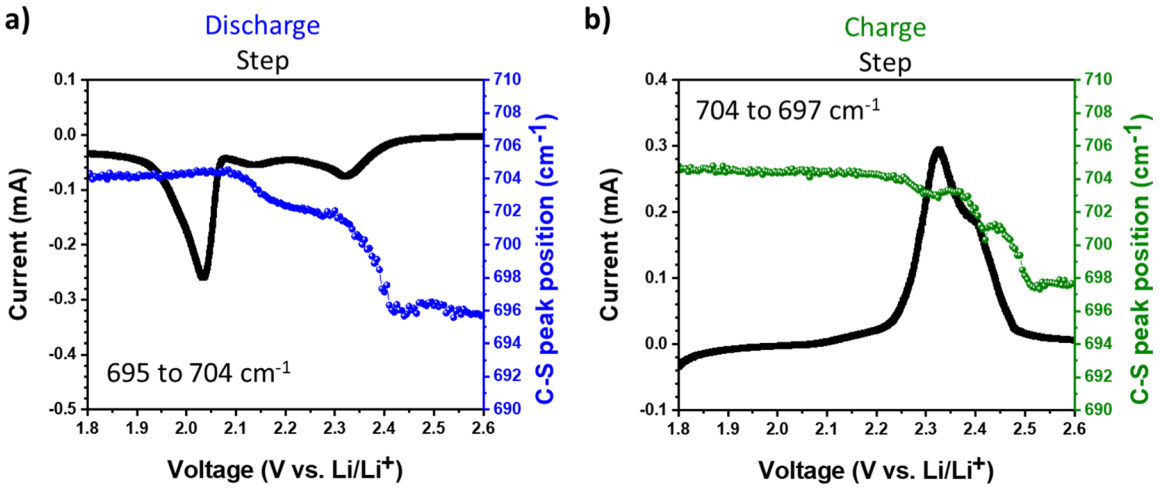

Figure 8. C−S peak evolution of the S80DIB20 in situ cell in the first (a) discharge step and (b) charge step.

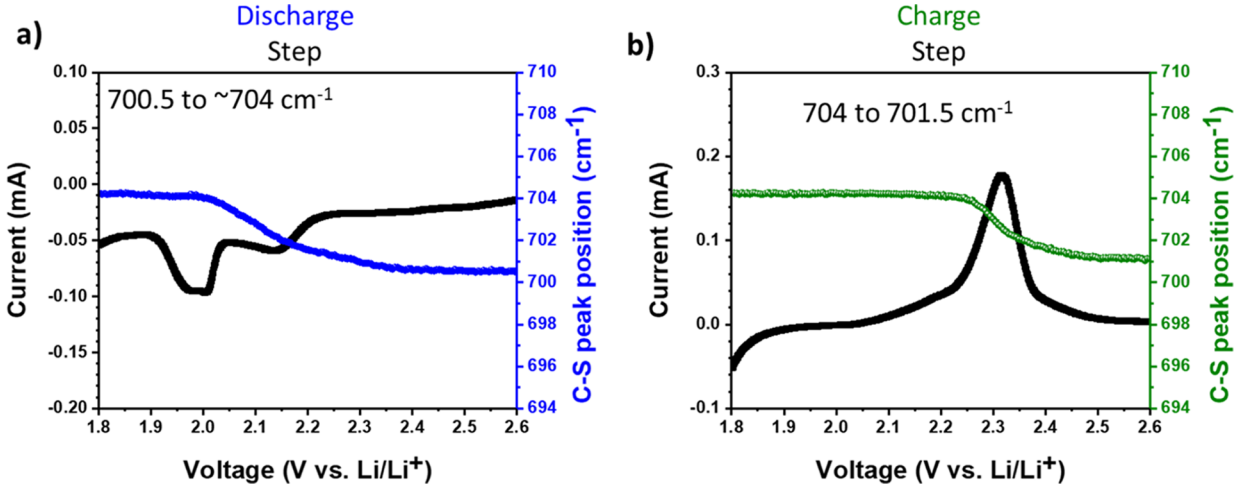

Figure 9. C−S peak evolution of the S30DIB70 in situ cell in the first (a) discharge strep and (b) charge step.

$$RSSR + 4Li^+ \leftrightarrow 2R + 2Li_2S \quad (2)$$

Note that in these equations, R is the organic part of the sulfur-rich copolymers, and it changes based on the monomer used in the reactions. In this work, R represents the DIB monomer used in the inverse vulcanization reaction; n is the sulfur chain length in the copolymer, also referred to as the sulfur bridging rank, in the current study. Based on the results provided so far, we concluded that the C−S bond in the sulfur copolymers is not electrochemically active in Li−S batteries. Therefore, we can conclude that reactions 1 and 2 proposed in several studies cannot represent the electrochemical behavior of the sulfur-rich copolymers. As a result, depending on the sulfur chain length in the copolymer, we propose that one of the following electrochemical reactions takes place in Li−S batteries with the sulfur copolymer active material.

High sulfur chain length, first discharge

$$RSS_nSR + (2n + 2)Li^+ + (2n + 2)e^- \rightarrow 2RSLi + nLi_2S \quad (3)$$

High sulfur chain length, subsequent charge and discharge

$$8mLi_2S \leftrightarrow 16mLi^+ + 16me^- + mS_8 \quad (4)$$

$$RSS_kSR + (2k + 2)Li^+ + (2k + 2)e^- \leftrightarrow 2RSLi + Li_2S \quad (5)$$

Low sulfur chain length

$$RSSR + 2Li^+ + 2e^- \leftrightarrow 2RSLi \quad (6)$$

It is worth mentioning that the based on these equations, the sulfur chain length determines the formation and amount of Li_2S at the end of discharge. If $n > 0$, then based on eq 3, b moles of Li_2S will be deposited as the discharge product. The formation of Li_2S will lead to formation of loose sulfur in the subsequent charge (eq 4). In addition, the sulfur chain length in the copolymer will change based on the amount of loose sulfur produced. In this regard, it is shown that having 38 wt % DIB in the SDIB copolymer is thermodynamically favorable DIB.[54] For low-sulfur chain length (where $n = 0$), the charge and discharge reaction pathways would follow eq 6, consequently, no Li_2S, and as a result, no loose sulfur is formed.

Moreover, another conclusion drawn from the study by Lee et al. using *ex situ* solid-state NMR was that the sulfur bridging rank remains constant at various cycles.[51] Based on their work, the discharge product of the SDIB copolymer is the lithium organo-polysulfide species along with Li_2S. In the charging step, they proposed that the SDIB copolymer with same sulfur

https://doi.org/10.1021/acs.jpcc.1c09124
J. Phys. Chem. C 2022, 126, 12327−12338

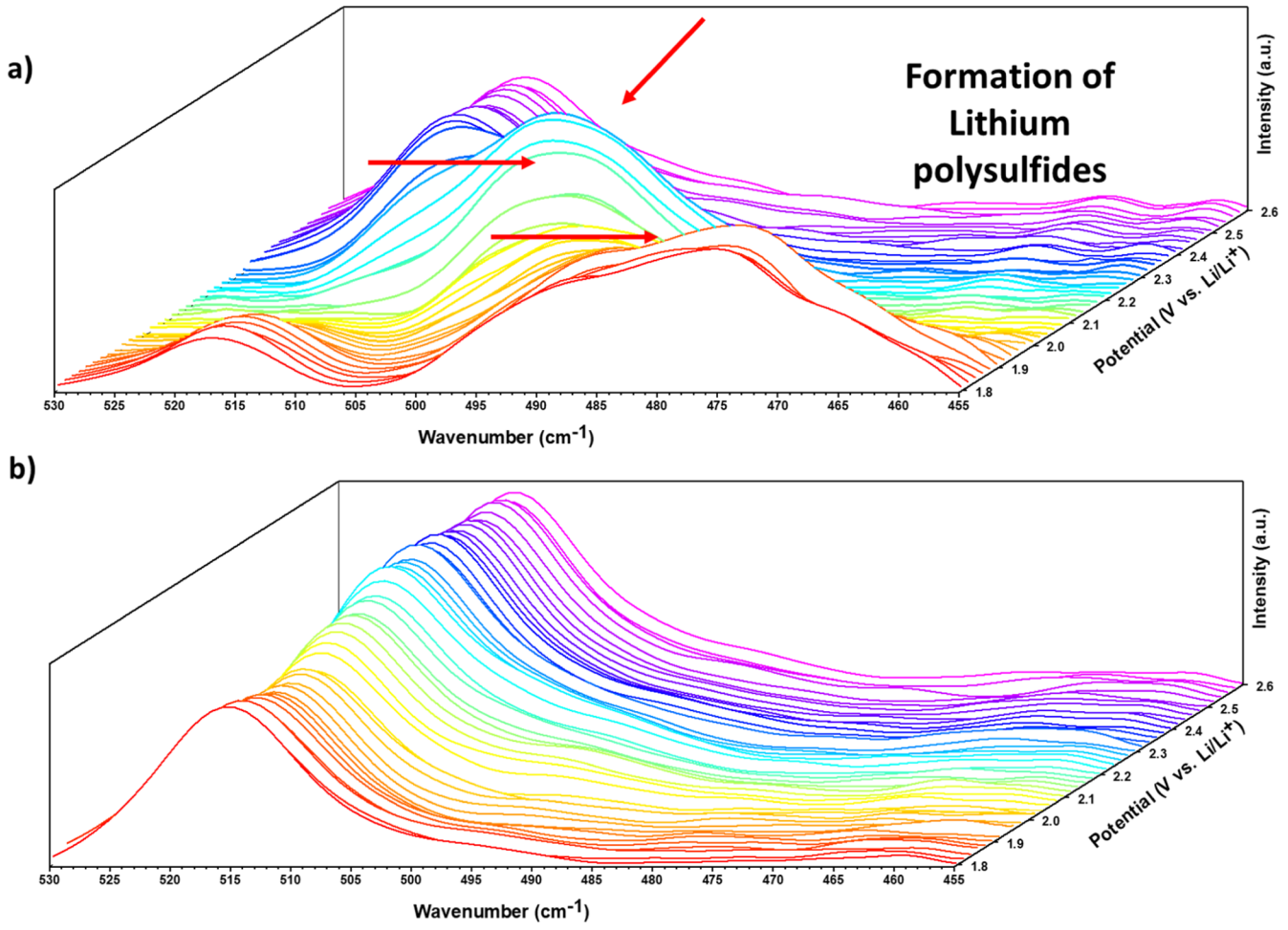

Figure 10. S−S peak evolution in the polysulfide region for the (a) S80DIB20 copolymer active material and (b) S30DIB70 active material.

bridging rank is formed, and overall, the electrochemical reaction in such copolymers is reversible. To investigate this claim, we have correlated the C−S bond peak position with the cell potential. To do so, we have extracted the C−S peak position from each spectrum at any given potential. The C−S peak position versus voltage for the first cycle for S80DIB20/CNF samples is presented in Figure 8a,b. As shown in these figures, for the discharge step, the C−S peak shifts from 695 to 704 cm^{-1}. On charging, this peak shifts back to 697 cm^{-1}. The cyclic shift confirms the S−S bond breakage within the sulfur bridging chains and the formation of organo-lithium polysulfides during reduction (discharge) and re-formation of the copolymer during oxidation (charge). However, these results also show that the C−S peak position does not fully recover after charging, which we believe, can be attributed to the formation of a copolymer with different sulfur chain lengths compared to the initial copolymer. A similar trend is observed for the second cycle (presented in Figure S6).

On the other hand, when S30DIB70, with presumably smaller sulfur chain length, is used as the active material, the C−S peak position shifted from 700.5 to 704 cm^{-1} only. Based on the results presented in Figure 9a,b, the C−S peak position at OCV in S30DIB70 (700 cm^{-1}) is considerably lower compared to that in S80DIB20 (695 cm^{-1}), confirming a significant decrease in the sulfur chain length and consequently a shorter-chained organo-polysulfide even at the start of the discharge. Moreover, the overall shift in the C−S peak position (3.5 cm^{-1}) is much lower than the S80DIB20 copolymers (9 cm^{-1}), another evidence for the presence of smaller sulfur bridging chain length at the start of discharge. This is consistent with the CV results that showed disappearance of the higher-order polysulfide peak. Figure S7 shows the C−S peak position of the S30DIB70 copolymer versus the cell voltage for the second cycle, confirming a similar trend and reversibility of the electrochemical reactions in this copolymer.

***In Operando* Study on Lithium Polysulfide Evolution in Sulfur Copolymers.** In this subsection, we investigate the evolution of the S−S bond in a region between 460 and 530 cm^{-1}. We believe that because of the long sulfur chain length in the S80DIB20, the formation of loose lithium polysulfide alongside the organo-lithium polysulfide would be inevitable. On the other hand, the disappearance of this peak in the S30DIB70 copolymer with significantly smaller sulfur chain length might arise from the elimination of long-chain polysulfide formation. Therefore, we monitored the S−S bond evolution in the region between 460 to 530 cm^{-1}. Figure 10a shows the *in operando* FTIR spectra of the S80DIB20 copolymer in this region. The peak at ∼517 cm^{-1} is assigned to $-CF_3$ bending from the electrolyte.[55] Therefore, this peak does not shift during reduction/oxidation and is independent of cell potential changes. However, as shown in Figure 10a, a new peak appears as the cell is discharged (highlighted with red arrows). Based on a previous study in our group and another study by Saqib et al., this new peak at ∼506 cm^{-1} is attributed

https://doi.org/10.1021/acs.jpcc.1c09124
J. Phys. Chem. C 2022, 126, 12327−12338

to the formation of higher-order lithium polysulfides.[50,56] This broad peak shifts to the lower wavenumbers as the cell is further discharged. This red shift in this region suggests further reduction of higher-order polysulfides to lower-order polysulfides. During discharge, as the sulfur chains become shorter, the polar Li terminal atoms get closer to the central S−S bond, thereby weakening the (S−S) bond strength. For the sake of comparison, we have provided the CV and *in operando* FTIR result of the cell with the S_8 active material (instead of SDIB) in Figure S8, which matches in trend with the SDIB spectra shown in Figure 10a. Based on this comparison, we can confirm that polysulfides are formed when a copolymer with high sulfur chain length is used. In the first discharge, the S−S bond cleavage takes place, according to eq 3, where organo lithium polysulfides are formed along with Li_2S. In the first charge, the formation of Li_2S results in formation of loose sulfur, and the sulfur chain length in sulfur-rich copolymer changes subsequently (eqs 4 and 5). The formation of loose sulfur and polysulfides results in formation of loose lithium polysulfides, as evident from the FTIR spectra of the S80DIB20 copolymer.

Figure 10b shows the *in operando* FTIR spectra for shorter sulfur bridging chain length copolymer, S30DIB70. It is evident from this figure that no polysulfide peak is observed in the polysulfide region, further corroborating that formation of polysulfides in S30DIB70 is eliminated. This finding is consistent with the CV curve, showing the absence of the 2.3 V peak. These results confirm that the S30DIB70 copolymer, benefiting from the low sulfur chain length, follows eq 6, where the sulfur copolymer is reduced to organo-lithium polysulfides in discharge and oxidizes to the same sulfur copolymer in the reverse reaction, with no loose sulfur/lithium polysulfides formed.

Another confirmation for this hypothesis is shown in Figure S8a−d, where the charge−discharge curves and cycling stability of the S80DIB20/CNF (Figure S8a) and S30DIB70/CNF (Figure S8b) copolymers are compared. As shown in this figure, the potential profiles of the S80DIB20/CNF cell are very similar to those of the pure sulfur, with a plateau at ∼2.3 V (vs Li/Li^+). On the other hand, this plateau is not found on the potential plateau of the S30DIB70/CNFs. Moreover, the cycling stability of the S80DIB20 active material, presented in Figure S8c, shows a relative cycling stability up to 650 cycles; however, the S30DIB70 copolymer remined stable up to more than 1500 cycles (Figure S8d). We believe that this remarkable improvement is related to the absence of loose lithium polysulfides in the S30DIB70 copolymers. It is also important to note that the relatively low capacity in S30DIB70 might be related to the lower sulfur wt % in the S30DIB70 copolymers. A detailed calculation of the theoretical capacities provided in the Supporting Information shows that the decreasing the sulfur chain length results in a lower Coulombic efficiency of the sulfur copolymer.

While we acknowledge that the capacity reported here is low compared to that of the sulfur cathode, however, we want to emphasize that cathode optimization in terms of contact between the active material and conductive carbon becomes more important using an active material with such a high monomer wt %. The result of this study provides fundamental understanding of the sulfur copolymers and paves the way to synthesize novel chemistries with different sulfur chain lengths. Depending on the application, moderate capacity and long cycle life can be advantageous, and a mechanism for tuning the capacity versus cycle life parameter has been shown.

Based on our results, the long sulfur briefing units between the organic moieties of the copolymer would inevitably result in formation of loose lithium polysulfides and their subsequent shuttling. On the other hand, a full sulfur immobilization can be realized through an optimization of the sulfur chain length in the S30DIB70 copolymer.

CONCLUSIONS

In summary, we have investigated the electrochemical behavior of sulfur-rich copolymers using *in operando* FTIR spectroscopy. To the best of our knowledge, this study is the first *in operando* work to understand the reaction mechanisms of sulfur copolymers. We demonstrated FTIR spectroscopy as a tool to investigate the cyclic changes in the C−S peak position and S−S bond stretching vibrations at different voltages within the voltage window of Li−S batteries for two different copolymers. Changing copolymer sulfur weight percent changed the sulfur bridge lengths between DIB monomers and had a significant effect on the CV results. The reduction peak at ∼2.3 V associated with formation of long-chain polysulfides present in S80DIB20 disappeared when S30DIB70 was used as the active material. Long-term cycling demonstrated that S30DIB70 had slower capacity fade in comparison to higher-weight-percentage copolymers. In situ IR revealed the presence of long and intermediary chain polysulfides in S80DIB20 during discharge that was not present in lower-weight-percentage copolymers. This leads us to conclude that longer sulfur bridge lengths lead to the formation of long-chain polysulfides which are soluble and lead to shuttling. In contrast the shorter sulfur bridge lengths of low weight percentage copolymers are unable to form soluble polysulfides. The reduction reaction of these shorter-chain length copolymers leads directly to solid Li_2S_2 and Li_2S_2 and with no intermediary polysulfides, leading to a lack of redox peak at ∼2.3 V, stable cycling for 1500 cycles, and no polysulfide signal in in situ IR. Moreover, comparing the FTIR results of S80DIB20 and S30DIB70 copolymers, we show that the C−S peak in these copolymer shifts to higher wavenumbers when the cell is discharged. The C−S peak shift is 9 cm^{-1} for the S80DIB20 copolymer. This shift decreases to 4 cm^{-1} for the S30DIB70 copolymer. The cleavage of intermediary S−S bonds in SDIB leads to the blue shift of the C−S peak. In SDIB copolymers with higher weight percentage of sulfur, this shift is larger due to the removal during discharge of a larger number of electronegative sulfur atoms and the strengthening of the C−S bond. In lower-weight-percent SDIB copolymers, the smaller sulfur bridge chain length both prevents the formation of soluble polysulfides and leads to a smaller shift in the peak position of the C−S bond. Additionally, in the S−S stretching region, several peaks appear for the S80DIB20 copolymer when the cell is discharged, while no peak is observed for S30DIB70. These two observations confirm that the polysulfide formation can be avoided by simply decreasing the sulfur wt % (or sulfur bridging length). By keeping sulfur bridge lengths less than four sulfur atoms long, the shuttle effect is mitigated via anchoring by inactive C−S bonds at the end of the chain and insolubility of the remaining one or two sulfur atom polysulfides in the middle of the chain. A stable cycle life of 1500 cycles was achieved when S30DIB70 was used as the active material.

https://doi.org/10.1021/acs.jpcc.1c09124
J. Phys. Chem. C 2022, 126, 12327−12338

■ ASSOCIATED CONTENT

Supporting Information

The Supporting Information is available free of charge at https://pubs.acs.org/doi/10.1021/acs.jpcc.1c09124.

Additional polymer characterization data, images of the synthesized organo-sulfur polymers, both optical and SEM and the DSC plots of the second and third heating cycles, blank cell in situ studies and CV and IR data, position of the C−S peak in the second cycle, cycling stability and voltage profiles for S80DIB20 and S30DIB70, XPS data demonstrating the presence of lithium sulfide, and theoretical capacity calculation (PDF)

■ AUTHOR INFORMATION

Corresponding Author

Vibha Kalra − *Chemical and Biological Engineering, Drexel University, Philadelphia 19104 Pennsylvania, United States;* orcid.org/0000-0002-2630-1560; Email: vk99@drexel.edu

Authors

Ayda Rafie − *Chemical and Biological Engineering, Drexel University, Philadelphia 19104 Pennsylvania, United States*

Rhyz Pereira − *Chemical and Biological Engineering, Drexel University, Philadelphia 19104 Pennsylvania, United States*

Ahmad Arabi Shamsabadi − *Chemistry Department, University of Pennsylvania, Philadelphia 19104 Pennsylvania, United States*

Complete contact information is available at: https://pubs.acs.org/10.1021/acs.jpcc.1c09124

Author Contributions

The manuscript was written through the contributions of all authors. All authors have approved the final version of the manuscript.

Funding

This work was funded by the National Science Foundation (NSF-1804374 and NSF- 1537827). A.A.S. was supported by a postdoctoral fellowship from the Vagelos Institute for Energy Science and Technology (VIEST).

Notes

The authors declare no competing financial interest.

■ ACKNOWLEDGMENTS

The authors acknowledge the Materials Characterization Core at Drexel University and The Laboratory for Research on the Structure of Matter at University of Pennsylvania for providing access to SEM and XRD systems, respectively. We would like to acknowledge Dr. Aaron Fafarman at Drexel University for his valuable comments and insight. We acknowledge Dr. Palmese's group at Drexel University for providing TGA and Dr. Fakhraai's Lab at the University of Pennsylvania for providing access to the DSC system.

■ REFERENCES

(1) Manthiram, A.; Fu, Y.; Chung, S.-H.; Zu, C.; Su, Y.-S. Rechargeable Lithium−Sulfur Batteries. *Chem. Rev.* **2014**, *114*, 11751−11787.

(2) Xu, R.; Lu, J.; Amine, K. Progress in Mechanistic Understanding and Characterization Techniques of Li-S Batteries. *Adv. Energy Mater.* **2015**, *5*, 1500408.

(3) Wild, M.; O'neill, L.; Zhang, T.; Purkayastha, R.; Minton, G.; Marinescu, M.; Offer, G. J. Lithium Sulfur Batteries, a Mechanistic Review. *Energy Environ. Sci.* **2015**, *8*, 3477−3494.

(4) Zhu, K.; Wang, C.; Chi, Z.; Ke, F.; Yang, Y.; Wang, A.; Wang, W.; Miao, L. How Far Away Are Lithium-Sulfur Batteries from Commercialization? *Front. Energy Res.* **2019**, *7*, 123.

(5) Li, T.; Bai, X.; Gulzar, U.; Bai, Y. J.; Capiglia, C.; Deng, W.; Zhou, X.; Liu, Z.; Feng, Z.; Proietti Zaccaria, R. A Comprehensive Understanding of Lithium−Sulfur Battery Technology. *Adv. Funct. Mater.* **2019**, *29*, 1901730.

(6) Fang, R.; Xu, J.; Wang, D.-W. Covalent Fixing of Sulfur in Metal−Sulfur Batteries. *Energy Environ. Sci.* **2020**, *13*, 432−471.

(7) Singh, A.; Rafie, A.; Kalra, V. Revisiting the Use of Electrolyte Additives in Li−S Batteries: The Role of Porosity of Sulfur Host Materials. *Sustain. Energy Fuels* **2019**, *3*, 2788−2797.

(8) Yang, W.; Yang, W.; Song, A.; Gao, L.; Sun, G.; Shao, G. Pyrrole as a Promising Electrolyte Additive to Trap Polysulfides for Lithium-Sulfur Batteries. *J. Power Sources* **2017**, *348*, 175−182.

(9) Rafie, A.; Pai, R.; Kalra, V. A Dual-Role Electrolyte Additive for Simultaneous Polysulfide Shuttle Inhibition and Redox Mediation in Sulfur Batteries. *J. Mater. Chem. A* **2021**, *9*, 26976−26988.

(10) Singhal, R.; Chung, S.-H.; Manthiram, A.; Kalra, V. A Free-Standing Carbon Nanofiber Interlayer for High-Performance Lithium−Sulfur Batteries. *J. Mater. Chem. A* **2015**, *3*, 4530−4538.

(11) Babu, G.; Sawas, A.; Thangavel, N. K.; Arava, L. M. R. Two-Dimensional Material-Reinforced Separator for Li−Sulfur Battery. *J. Phys. Chem. C* **2018**, *122*, 10765−10772.

(12) He, Y.; Wu, S.; Li, Q.; Zhou, H. Designing a Multifunctional Separator for High-Performance Li−S Batteries at Elevated Temperature. *Small* **2019**, *15*, 1904332.

(13) Ji, X.; Lee, K. T.; Nazar, L. F. A Highly Ordered Nanostructured Carbon−Sulphur Cathode for Lithium−Sulphur Batteries. *Nat. Mater.* **2009**, *8*, 500−506.

(14) Wang, M.; Xia, X.; Zhong, Y.; Wu, J.; Xu, R.; Yao, Z.; Wang, D.; Tang, W.; Wang, X.; Tu, J. Porous Carbon Hosts for Lithium−Sulfur Batteries. *Chem. - Eur. J.* **2019**, *25*, 3710−3725.

(15) Xiao, Z.; Li, Z.; Meng, X.; Wang, R. Mxene-Engineered Lithium−Sulfur Batteries. *J. Mater. Chem. A* **2019**, *7*, 22730−22743.

(16) Zhang, C.; Cui, L.; Abdolhosseinzadeh, S.; Heier, J. Two-Dimensional Mxenes for Lithium-Sulfur Batteries. *InfoMat* **2020**, *2*, 613−638.

(17) Seh, Z. W.; Li, W.; Cha, J. J.; Zheng, G.; Yang, Y.; McDowell, M. T.; Hsu, P.-C.; Cui, Y. Sulphur−Tio 2 Yolk−Shell Nano-architecture with Internal Void Space for Long-Cycle Lithium−Sulphur Batteries. *Nat. Commun.* **2013**, *4*, 1331.

(18) Li, Q.; Ma, Z.; Li, J.; Liu, Z.; Fan, L.; Qin, X.; Shao, G. Core−Shell-Structured Sulfur Cathode: Ultrathin Δ-Mno2 Nanosheets as the Catalytic Conversion Shell for Lithium Polysulfides in High Sulfur Content Lithium−Sulfur Batteries. *ACS Appl. Mater. Interfaces* **2020**, *12*, 35049−35057.

(19) Robinson, J. B.; Xi, K.; Kumar, R. V.; Ferrari, A. C.; Au, H.; Titirici, M.-M.; Parra-Puerto, A.; Kucernak, A.; Fitch, S. D. S.; Garcia-Araez, N.; Brown, Z. L.; Pasta, M.; Furness, L.; Kibler, A. J.; Walsh, D. A.; Johnson, L. R.; Holc, C.; Newton, G. N.; Champness, N. R.; Markoulidis, F.; Crean, C.; Slade, R. C. T.; Andritsos, E. I.; Cai, Q.; Babar, S.; Zhang, T.; Lekakou, C.; Kulkarni, N.; Rettie, A. J. E.; Jervis, R.; Cornish, M.; Marinescu, M.; Offer, G.; Li, Z.; Bird, L.; Grey, C. P.; Chhowalla, M.; Lecce, D. D.; Owen, R. E.; Miller, T. S.; Brett, D. J. L.; Liatard, S.; Ainsworth, D.; Shearing, P. R. 2021 Roadmap on Lithium Sulfur Batteries. *J. Phys.: Energy* **2021**, *3*, 031501.

(20) Zeng, Z.; Liu, X. Sulfur Immobilization by "Chemical Anchor" to Suppress the Diffusion of Polysulfides in Lithium−Sulfur Batteries. *Adv. Mater. Interfaces* **2018**, *5*, 1701274.

(21) Li, M.; Wang, Y.; Sun, S.; Yang, Y.; Gu, G.; Zhang, Z. Rational Design of an Allyl-Rich Triazine-Based Covalent Organic Framework Host Used as Efficient Cathode Materials for Li-S Batteries. *Chem. Eng. J.* **2022**, *429*, 132254.

(22) Shi, K.; Lin, Y.; Li, J.; Xiong, Z.; Liao, J.; Liu, Q. Fabrication and Porous Architecture of Crosslinked Polyimides for Lithium−

Sulfur Batteries and Their Electrochemical Properties. *Ind. Eng. Chem. Res.* **2022**, *61*, 2502.
(23) Bhargav, A.; Ma, Y.; Shashikala, K.; Cui, Y.; Losovyj, Y.; Fu, Y. The Unique Chemistry of Thiuram Polysulfides Enables Energy Dense Lithium Batteries. *J. Mater. Chem. A* **2017**, *5*, 25005−25013.
(24) Wei, S.; Ma, L.; Hendrickson, K. E.; Tu, Z.; Archer, L. A. Metal−Sulfur Battery Cathodes Based on Pan−Sulfur Composites. *J. Am. Chem. Soc.* **2015**, *137*, 12143−12152.
(25) Li, X.; Liang, J.; Lu, Y.; Hou, Z.; Cheng, Q.; Zhu, Y.; Qian, Y. Sulfur-Rich Phosphorus Sulfide Molecules for Use in Rechargeable Lithium Batteries. *Angew. Chem., Int. Ed.* **2017**, *56*, 2937−2941.
(26) Cui, Y.; Abouimrane, A.; Lu, J.; Bolin, T.; Ren, Y.; Weng, W.; Sun, C.; Maroni, V. A.; Heald, S. M.; Amine, K. (De) Lithiation Mechanism of Li/Ses X (X= 0−7) Batteries Determined by in Situ Synchrotron X-Ray Diffraction and X-Ray Absorption Spectroscopy. *J. Am. Chem. Soc.* **2013**, *135*, 8047−8056.
(27) Cui, Y.; Ackerson, J. D.; Ma, Y.; Bhargav, A.; Karty, J. A.; Guo, W.; Zhu, L.; Fu, Y. Phenyl Selenosulfides as Cathode Materials for Rechargeable Lithium Batteries. *Adv. Funct. Mater.* **2018**, *28*, 1801791.
(28) Chung, W. J.; Griebel, J. J.; Kim, E. T.; Yoon, H.; Simmonds, A. G.; Ji, H. J.; Dirlam, P. T.; Glass, R. S.; Wie, J. J.; Nguyen, N. A.; Guralnick, B. W.; Park, J.; Somogyi, Á.; Theato, P.; Mackay, M. E.; Sung, Y.-E.; Char, K.; Pyun, J. The Use of Elemental Sulfur as an Alternative Feedstock for Polymeric Materials. *Nat. Chem.* **2013**, *5*, 518−524.
(29) Xiao, J.; Liu, Z.; Zhang, W.; Deng, N.; Liu, J.; Zhao, F. Inverse Vulcanization of a Natural Monoene with Sulfur as Sustainable Electrochemically Active Materials for Lithium-Sulfur Batteries. *Molecules* **2021**, *26*, 7039.
(30) Simmonds, A. G.; Griebel, J. J.; Park, J.; Kim, K. R.; Chung, W. J.; Oleshko, V. P.; Kim, J.; Kim, E. T.; Glass, R. S.; Soles, C. L.; Sung, Y.-E.; Char, K.; Pyun, J. Inverse Vulcanization of Elemental Sulfur to Prepare Polymeric Electrode Materials for Li−S Batteries. *ACS Macro Lett.* **2014**, *3*, 229−232.
(31) Hu, G.; Sun, Z.; Shi, C.; Fang, R.; Chen, J.; Hou, P.; Liu, C.; Cheng, H.-M.; Li, F. A Sulfur-Rich Copolymer@ Cnt Hybrid Cathode with Dual-Confinement of Polysulfides for High-Performance Lithium−Sulfur Batteries. *Adv. Mater.* **2017**, *29*, 1603835.
(32) Ma, J.; Fan, J.; Chen, S.; Yang, X.; Hui, K. N.; Zhang, H.; Bielawski, C. W.; Geng, J. Covalent Confinement of Sulfur Copolymers onto Graphene Sheets Affords Ultrastable Lithium−Sulfur Batteries with Fast Cathode Kinetics. *ACS Appl. Mater. Interfaces* **2019**, *11*, 13234−13243.
(33) Choudhury, S.; Srimuk, P.; Raju, K.; Tolosa, A.; Fleischmann, S.; Zeiger, M.; Ozoemena, K. I.; Borchardt, L.; Presser, V. Carbon Onion/Sulfur Hybrid Cathodes Via Inverse Vulcanization for Lithium−Sulfur Batteries. *Sustain. Energy Fuels* **2018**, *2*, 133−146.
(34) Zhang, Y.; Griebel, J. J.; Dirlam, P. T.; Nguyen, N. A.; Glass, R. S.; Mackay, M. E.; Char, K.; Pyun, J. Inverse Vulcanization of Elemental Sulfur and Styrene for Polymeric Cathodes in Li-S Batteries. *J. Polym. Sci., Part A: Polym. Chem.* **2017**, *55*, 107−116.
(35) Gomez, I.; Mecerreyes, D.; Blazquez, J. A.; Leonet, O.; Ben Youcef, H.; Li, C.; Gómez-Cámer, J. L.; Bondarchuk, O.; Rodriguez-Martinez, L. Inverse Vulcanization of Sulfur with Divinylbenzene: Stable and Easy Processable Cathode Material for Lithium-Sulfur Batteries. *J. Power Sources* **2016**, *329*, 72−78.
(36) Dirlam, P. T.; Simmonds, A. G.; Kleine, T. S.; Nguyen, N. A.; Anderson, L. E.; Klever, A. O.; Florian, A.; Costanzo, P. J.; Theato, P.; Mackay, M. E.; Glass, R. S.; Char, K.; Pyun, J. Inverse Vulcanization of Elemental Sulfur with 1, 4-Diphenylbutadiyne for Cathode Materials in Li−S Batteries. *RSC Adv.* **2015**, *5*, 24718−24722.
(37) Bayram, O.; Kiskan, B.; Demir, E.; Demir-Cakan, R.; Yagci, Y. Advanced Thermosets from Sulfur and Renewable Benzoxazine and Ionones Via Inverse Vulcanization. *ACS Sustainable Chem. Eng.* **2020**, *8*, 9145−9155.
(38) Wang, Y.; Zhou, D.; Wang, G. Sulfur-Containing Polymer Cathode Materials for Li−S Batteries. *Advances in Rechargeable Lithium−Sulfur Batteries*; Springer Nature, 2022; pp 295−330.
(39) Shen, J.; Feng, Y.; Wang, P.; Qiu, G.; Zhang, L.; Lu, L.; Wang, H.; Wang, R.; Linkov, V.; Ji, S. Conductive Sulfur-Rich Copolymer Composites as Lithium−Sulfur Battery Electrodes with Fast Kinetics and a High Cycle Stability. *ACS Sustainable Chem. Eng.* **2020**, *8*, 10389−10401.
(40) Yang, Y.; Zhu, Y.; Raju, K.; Dai, S.; Jafta, C. J. Recent in Situ/Operando Characterization of Lithium-Sulfur Batteries. *Nanostructured Materials for Energy Related Applications*; Springer, 2019; pp 21−40.
(41) Tan, J.; Liu, D.; Xu, X.; Mai, L. In Situ/Operando Characterization Techniques for Rechargeable Lithium−Sulfur Batteries: A Review. *Nanoscale* **2017**, *9*, 19001−19016.
(42) Rafie, A.; Singh, A.; Kalra, V. Synergistic Effect of Sulfur-Rich Copolymer/S8 and Carbon Host Porosity in Li-S Batteries. *Electrochim. Acta* **2021**, *365*, 137088.
(43) Zhang, S. Understanding of Sulfurized Polyacrylonitrile for Superior Performance Lithium/Sulfur Battery. *Energies* **2014**, *7*, 4588−4600.
(44) Wu, Z.; Bak, S.-M.; Shadike, Z.; Yu, S.; Hu, E.; Xing, X.; Du, Y.; Yang, X.-Q.; Liu, H.; Liu, P. Understanding the Roles of the Electrode/Electrolyte Interface for Enabling Stable Li‖ Sulfurized Polyacrylonitrile Batteries. *ACS Appl. Mater. Interfaces* **2021**, *13*, 31733.
(45) Kim, H.; Kim, C.; Sadan, M. K.; Yeo, H.; Cho, K.-K.; Kim, K.-W.; Ahn, J.-H.; Ahn, H.-J. Binder-Free and High-Loading Sulfurized Polyacrylonitrile Cathode for Lithium/Sulfur Batteries. *RSC Adv.* **2021**, *11*, 16122−16130.
(46) Li, H.; Xue, W.; Wang, L.; Liu, T. Two Competing Reactions of Sulfurized Polyacrylonitrile Produce High-Performance Lithium−Sulfur Batteries. *ACS Appl. Mater. Interfaces* **2021**, *13*, 25002.
(47) Hanwell, M. D.; Curtis, D. E.; Lonie, D. C.; Vandermeersch, T.; Zurek, E.; Hutchison, G. R. Avogadro: An Advanced Semantic Chemical Editor, Visualization, and Analysis Platform. *J. Cheminf.* **2012**, *4*, 17.
(48) Dillard, C.; Chung, S.-H.; Singh, A.; Manthiram, A.; Kalra, V. Binder-Free, Freestanding Cathodes Fabricated with an Ultra-Rapid Diffusion of Sulfur into Carbon Nanofiber Mat for Lithiumsulfur Batteries. *Materials Today Energy* **2018**, *9*, 336−344.
(49) Shankarayya Wadi, V. K.; Jena, K. K.; Khawaja, S. Z.; Yannakopoulou, K.; Fardis, M.; Mitrikas, G.; Karagianni, M.; Papavassiliou, G.; Alhassan, S. M. NMR and EPR Structural Analysis and Stability Study of Inverse Vulcanized Sulfur Copolymers. *ACS Omega* **2018**, *3*, 3330−3339.
(50) Dillard, C.; Singh, A.; Kalra, V. Polysulfide Speciation and Electrolyte Interactions in Lithium−Sulfur Batteries with in Situ Infrared Spectroelectrochemistry. *J. Phys. Chem. C* **2018**, *122*, 18195−18203.
(51) Hoefling, A.; Nguyen, D. T.; Partovi-Azar, P.; Sebastiani, D.; Theato, P.; Song, S.-W.; Lee, Y. J. Mechanism for the Stable Performance of Sulfur-Copolymer Cathode in Lithium−Sulfur Battery Studied by Solid-State Nmr Spectroscopy. *Chem. Mater.* **2018**, *30*, 2915−2923.
(52) Griebel, J. J.; Nguyen, N. A.; Astashkin, A. V.; Glass, R. S.; Mackay, M. E.; Char, K.; Pyun, J. Preparation of Dynamic Covalent Polymers Via Inverse Vulcanization of Elemental Sulfur. *ACS Macro Lett.* **2014**, *3*, 1258−1261.
(53) Zhang, S. S. Sulfurized Carbon: A Class of Cathode Materials for High Performance Lithium/Sulfur Batteries. *Front. Energy Res.* **2013**, *1*, 10.
(54) Kiani, R.; Sebastiani, D.; Partovi-Azar, P. On the Structure of Sulfur/1, 3-Diisopropenylbenzene Co-Polymer Cathodes for Li-S Batteries: Insights from Density-Functional Theory Calculations. *ChemPhysChem* **2022**, *23*, No. e202100519.
(55) Radziuk, D. V.; Möhwald, H. Spectroscopic Investigation of Composite Polymeric and Monocrystalline Systems with Ionic Conductivity. *Polymers* **2011**, *3*, 674−692.
(56) Saqib, N.; Ohlhausen, G. M.; Porter, J. M. In Operando Infrared Spectroscopy of Lithium Polysulfides Using a Novel Spectro-Electrochemical Cell. *J. Power Sources* **2017**, *364*, 266−271.

https://doi.org/10.1021/acs.jpcc.1c09124
J. Phys. Chem. C 2022, 126, 12327−12338